ChemComm

Accepted Manuscript

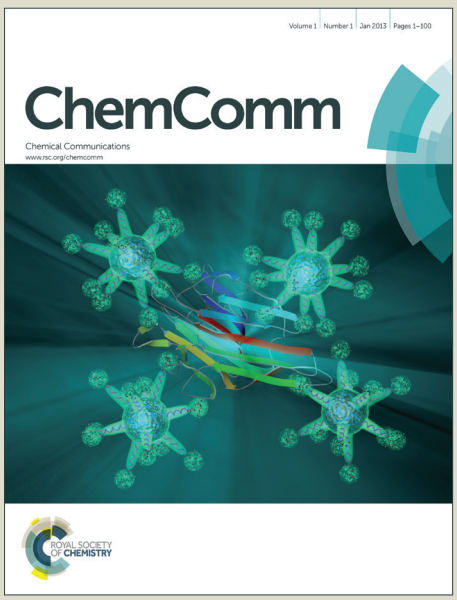

ROYAL SOCIETY OF CHEMISTRY

www.rsc.org/chemcomm

Journal Name

RSCPublishing

COMMUNICATION

Nanoparticle-electrode collisions as a dynamic seeding route for the growth of metallic nanostructures

Cite this: DOI: 10.1039/x0xx00000x

Andrew Pearson[a] and Anthony P. O'Mullane[b,*]

Received 00th January 2012,
Accepted 00th January 2012

DOI: 10.1039/x0xx00000x

www.rsc.org/

The collisions between colloidal metal nanoparticles and a carbon electrode were explored as a dynamic method for the electrodeposition of a diverse range of electrocatalytically active Ag and Au nanostructures whose morphology is dominated by the electrostatic interaction between the charge of the nanoparticle and metal salt.

Metal nanoparticle research is a mature field which has attracted the attention of synthetic, physical, materials and applied chemists. This is due to their fascinating size and shape dependent physical and chemical properties which are of fundamental interest but also applicable in catalysis, electrocatalysis, surface enhanced Raman spectroscopy (SERS) based sensing and medical technology.[1] Of other interest is investigating the interaction of NPs with their environment which is important as these materials are gaining momentum in their commercial use as well as their proposed utilisation in medical applications within the body. In particular for the latter case the environment will be highly charged and electrostatic interactions will play a significant role in their applicability and activity. A particularly interesting subset of nanomaterials is two dimensional dendritic nanostructures which are highly branched and offer increased surface areas for the benefit of the aforementioned applications.[2] These structures are most often formed under non-equilibrium conditions where their formation is governed by diffusion limited or reaction limited aggregation.[2a] The field of electrochemistry offers significant benefits not only in terms of synthesis, where the size and shape of nanomaterials can be controlled, but also characterisation of the final material. This has allowed shape and size dependent electrocatalytic properties to be investigated at spheres, cubes, prisms, rods and dendrites.[1f, 3] In general, electrochemistry is undertaken at nanoparticles immobilised on support electrodes. However, in recent years, research initiated by Bard *et al*[4] and further developed by Compton *et al*[5] has explored collisions between colloidal nanoparticles and an inert electrode as a means to characterise metal nanoparticles such as Ag and Au.[4a, 4b] Moreover, recent advances in nanoparticle-impact electrochemistry have demonstrated that nanoparticle collisions can determine properties such as concentration, size and electron transfer kinetics.[5b, 6] Furthermore, collisions between graphite nanosheets with attached protein molecules and an electrode have aided with the detection of single protein molecules.[7] However, to date the concept of using nanoparticle collisions to direct the growth of materials on the surface of an electrode has yet to be explored. In this communication we demonstrate a proof of concept that nanoparticle collisions at a glassy carbon (GC) electrode during the electrodeposition of Ag and Au enables hierarchical dendritic nanostructures as well as isolated metal nanoparticles to be formed which is dependent on the electrostatic interaction between the nanoparticle and metal salt in solution. The electrocatalytic activity of the nanostructures is then explored via hydrazine oxidation.

Initially, the electrodeposition of Ag was carried out in a solution of 1 mM $AgNO_3$ in the absence of Ag nanoparticles at a potential of -0.10 V vs Ag/AgCl for 300s. The SEM image (Fig. 1A) shows that micrometre sized polygonal clusters are created over the GC surface where each cluster consists of crystallites of different sizes and shapes (inset Fig. 1A). However when tyrosine capped Ag nanoparticles (Ag-tyr) (see supplementary information for synthesis conditions and TEM images (Fig. S1A)) are introduced into the electrolyte the morphology of the deposit changes dramatically. The concentration of NPs is the equivalent concentration of Ag^+ or Au^{3+} used to prepare the NPs. With the addition of 50 μM Ag-tyr NPs the deposit consists of isolated dendritic clusters (Fig. 1B) with sub 100 nm features at the tips where the inset shows the growth originating from a central spherical particle which is consistent with the size of the Ag NPs used, i.e. 20 nm (Fig. S1A). When the concentration of Ag-tyr nanoparticles was increased to 500 μM (Fig. 1C), the deposited nanostructures demonstrated an intriguing sprawling fractal morphology, with sub 50 nm features at the tips. Furthermore the surface of the fractal nanostructures appear to be dotted with Ag nanoparticles, consistent with the size used in the experiment, which likely act as seeds for further growth. This hypothesis was confirmed by undertaking the experiment in the absence of $AgNO_3$ in solution under identical conditions, i.e. at an applied potential of -0.1 V (Fig. S2A). The formation of non-agglomerated Ag-tyr NPs on the electrode surface is evident which indicates that Ag NPs impact and then stick on the electrode surface. Increasing the concentration of Ag-tyr nanoparticles to 1 mM (Fig. 1D) did not continue the trend of anisotropic growth but rather in the formation of discreet, irregular nanoclusters of Ag between 50 nm and 100 nm in diameter.

When we next consider the electrodeposition of Au nanostructures in the absence and presence of citrate capped Au

nanoparticles (Au-cit) (supplementary information for synthesis conditions and TEM images (Fig. S1B)), we observe a stark difference in behaviour (Fig. 1E-H), compared to the Ag case. When Au is electrodeposited from 1 mM $HAuCl_4$ at 0.30 V vs Ag/AgCl for 300s in the absence of Au-cit NPs a sparse coverage of irregular spheroidal shaped micrometre sized clusters consisting of numerous smaller particles was found (Fig. 1E and inset). When electrodeposition was carried out with 50 μM Au-cit NPs in solution (Fig. 1F) the Au cluster size with respect to the control material (Fig. 1E) was reasonably consistent, however the morphology of the Au clusters was quite different and consisted of more closely packed small crystallites. Significantly, electrodeposition with 500 μM Au-cit NPs (Fig. 1G) results in the formation of sub 100 nm Au nanoclusters that are well dispersed across the surface, in contrast to the larger clusters observed with the 50 μM Au-cit NP concentration.

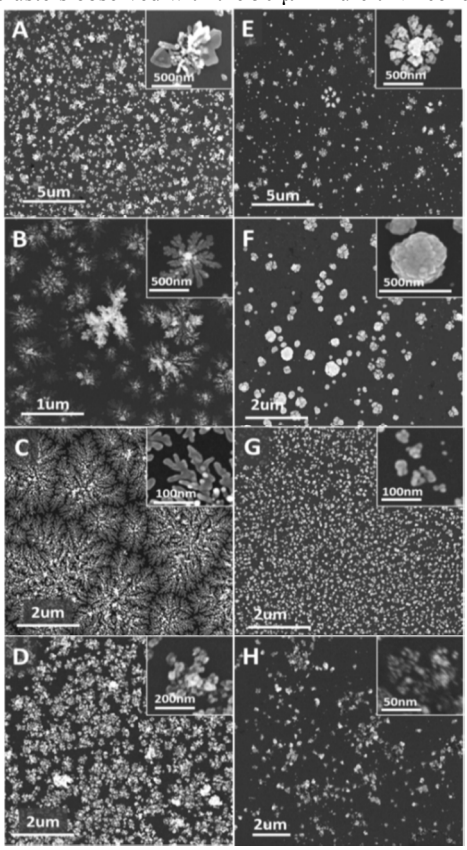

Figure 1. SEM images of electrodeposited nanostructures using $AgNO_3$ with (A) no Ag-tyr, (B) 50 μM, (C) 500 μM and (D) 1 mM Ag-tyr or $[AuCl_4]^-$ with (E) no Au-cit, (F) 50 μM, (G) 500 μM and (H) 1 mM Au-cit.

Finally, electrodeposition in the presence of 1 mM Au-cit NPs (Fig. 1H) results in a more sparsely covered electrode surface consisting of small nanostructures of ca. 20 nm in diameter which is consistent with the size of the Au-cit NPs (Fig. S1B). The control experiment in the absence of $HAuCl_4$ also shows that Au NPs impact and stick on the electrode surface under these conditions (Fig. S2B).

We attribute this difference in morphology between the Ag and Au systems (fractal versus well dispersed clusters) to the influence of the electrostatic charge on the respective metal ions and nanoparticles in solution. Both Ag-tyr and Au-cit NPs possess functional groups which will exhibit a negative surface charge in aqueous solution that will attract Ag^+ ions and repel $[AuCl_4]^-$ ions respectively at the nanoparticle surface. By attracting the Ag^+ ions towards the Ag-tyr nanoparticles that are impacting the electrode surface the growth of large fractal structures is promoted (Fig. 1B and 1C) until a point where the excessive abundance of Ag-tyr nanoparticles eventually leads to significant agglomeration and the formation of irregular clusters (Fig. 1D). Furthermore, when we consider that negative $[AuCl_4]^-$ ions will be repelled from the Au-cit NPs at the electrode surface due to their negative surface charge then the formation of isolated clusters is not surprising.

Fig. 2A shows linear sweep voltammograms (LSV) recorded in 1 mM $AgNO_3$ at a GC electrode and different concentrations of Ag-tyr nanoparticles that correspond to the electroreduction of Ag^+ to Ag^0 at the GC surface. Also shown is a LSV recorded in just a Ag NP solution without $AgNO_3$ which demonstrates only double layer charging of the GC electrode in the potential range of interest. Immediately apparent is the shift in peak current position to more negative values with increasing Ag-tyr NP concentration, however the magnitude of the current is only slightly diminished. Significantly different behaviour was observed for Au electrodeposition in the presence of Au-cit NPs (Fig. 2B). There is a large decrease in current magnitude upon the introduction of Au-cit NPS to the 1 mM $HAuCl_4$ electrolyte as well as a similar shift in peak potential to less positive values, as in the Ag case, where the former in particular indicates significant inhibition of Au electrodeposition.

Fig. 2C and D show the chronoamperometric data for the synthesis of Ag and Au nanostructures as seen in Fig. 1. The deposition potentials were chosen beyond the peak potentials for both Ag and Au deposition to ensure comparability of the two systems. For the case of Au deposition the current being passed decreases in comparison to the case with no NPs present upon the addition of Au NPs. For the case of Ag deposition there is also a lower current passed except for when 500 μM Ag-tyr NPs are present in solution which shows an increased current compared to the case where no NPs are present. Interestingly this corresponds to the formation of highly dendritic Ag nanostructures over the entire substrate as seen in Fig. 1C. It is clear in the case of Au deposition that electrostatic repulsion between Au-cit NPs and $[AuCl_4]^-$ is a significant factor. However for the Ag case the data suggests that there may be more than just an electrostatic effect.

Previous studies have shown that the $[Fe(CN)_6]^{3-} + e^- \leftrightarrow [Fe(CN)_6]^{4-}$ process was affected by the presence of Au NPs, although the capping agent was not specified.[8] It was reported that the apparent diffusion coefficient of the redox species was lowered which resulted in lower currents. This was attributed to a blocking effect where the nanoparticles impeded the diffusion of the redox species to the electrode surface. This is because the Brownian motion of the nanoparticle is much less than the drift velocity of redox active species which then simply bounces back from the direction of the electrode. This was confirmed here with citrate capped Au NPs for ferrocyanide and ferrocenemethanol oxidation (supplementary section – Fig. S3). In the electrodeposition system under study here such a blocking effect would also operate, however it becomes more pronounced in the case of Au deposition where electrostatic repulsion effects will contribute to a significant extent and hence impede further the diffusion of $[AuCl_4]^-$ ions to the electrode surface and explains the observed dramatic decrease in electoreduction currents upon the introduction of higher concentrations of Au-cit NPs (Fig. 2B). For the Ag case this blocking effect will also operate but will be minimised due to the electrostatic attraction of Ag^+ cations to the negatively charged Ag-tyr NPs which for the 500 μM Ag-tyr case results in an increase in electroreduction current. This suggests that as well as free Ag^+ ions, those bound electrostatically to the Ag-tyr nanoparticles that are impacting on the electrode surface are also reduced. However at the higher concentration of 1 mM Ag-tyr the physical blocking effect

appears to dominate and results in lower deposition current and therefore less surface coverage (Fig. 1D).

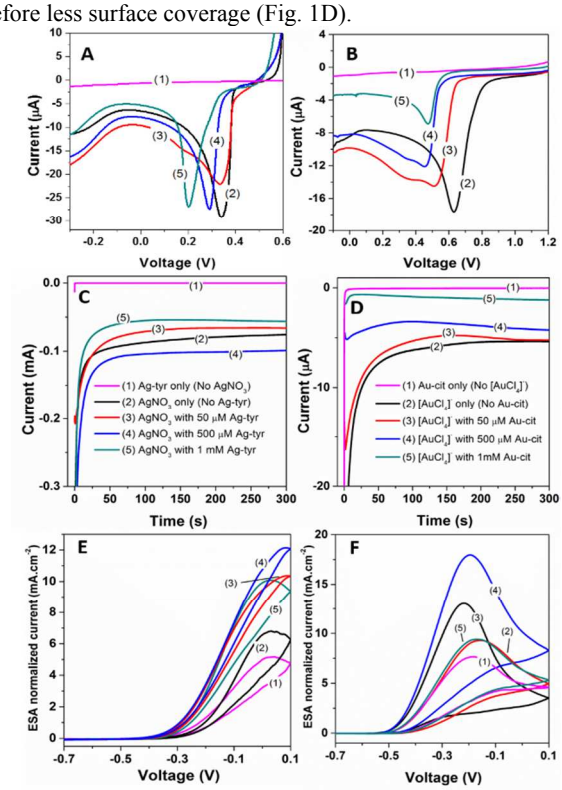

Figure 2. (A,B) LSVs obtained for the Ag (C) and Au (D) systems with and without NPs, recorded at 50 mVs^{-1} (C,D) CAs obtained at -100 mV for Ag (A) and 300 mV for Au (B) over 300 s. (E,F) CVs obtained at Ag (E) and Au (F) nanostructures in 50 mM hydrazine in 1 M NaOH, recorded at 50 mVs^{-1}.

The formation of Ag dendrites under electrochemical conditions is generally governed by a diffusion limited aggregation (DLA) model.[2a] When the applied potential is near the equilibrium potential for metal deposition, isolated nanoparticles are generated that often have a polygonal shape which was recently reported for Ag deposition[2c] and is consistent with Fig. 1A. When more negative potentials are applied, non-equilibrium conditions are induced where the diffusion of Ag^+ ions becomes the rate limiting step and dendrite formation occurs due to transport limited deposition. Under such non-equilibrium conditions the DLA growth model operates. Recently, Zhu *et al.*[2a] reported that Pd dendrites could be electrodeposited in a thin layer cell configuration to facilitate TEM imaging because the diffusion of Pd^{2+} became limited within such a confined geometry. However the DLA model usually accounts for a very open dendritic structure.[9] In Fig. 1C a very compact layer of dendrites is formed. The time evolution study (Fig. S4) shows that isolated dendritic microclusters are formed at short times (60 s) which grow together (300 s) and finally results in the growth of dendrites on top of the initial layer on the surface (1000 s). It should be noted in the absence of Ag-tyr NPs only a few dendritic crystals are formed after 1000 s (Fig. S4E). We propose that the DLA model does not operate under the conditions employed here with nanoparticles in solution. For the case of Au deposition the electrodeposition rate is severely inhibited (Fig. 2D) which indicates that the diffusion of $[AuCl_4]^-$ is inhibited which therefore should favour conditions for dendrite formation, however well isolated nanoparticles of Au are formed. Therefore we propose in the Ag case that the continuous impact of Ag NPs on the surface which is a random process creates a continuous source of nucleation sites upon which Ag can deposit. This random creation of nucleation sites is beneficial to aggregate formation that leads to dendritic growth over the entire surface. This does not happen in the Au case as the impacting nanoparticles repel the incoming $[AuCl_4]^-$ ions thereby inhibiting growth. This mechanism is illustrated in Scheme 1.

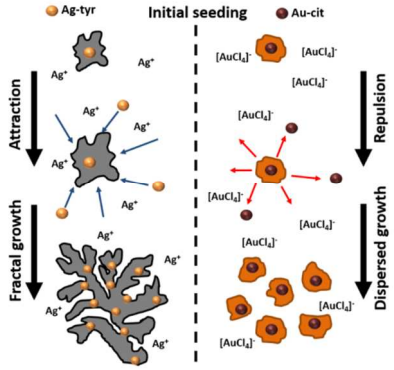

Scheme 1. Schematic representation of the growth process of fractal Ag structures and dispersed Au structures electrodeposited in the presence of Ag-tyr and Au-cit nanoparticles, respectively.

To test this hypothesis the electrode potential was made more negative to -0.30 V in the presence of 500 μM Ag-cit NPs which did not result in Ag dendrite formation (Fig. S4C). At this more negative electrode potential the electrostatic repulsion of negatively charged Ag-tyr from the electrode surface would occur which shuts off the formation of many nucleation centres upon which Ag dendrites can grow. It should be noted that an applied potential of -0.30 V is not sufficient to induce dendrite formation as shown by the control experiment in the absence of Ag NPs (Fig. S5C). In fact the 2 samples prepared at this applied potential in the presence and absence of Ag-tyr NPs, are remarkably similar. The role of tyrosine was also investigated where electrodeposition was carried out in an electrolyte containing 1 mM $AgNO_3$ and 0.5 mM tyrosine. The LSV data (Figure S6A) shows significant inhibition of the electrodeposition process which is evident by the much later onset potential and broad response with reduced current magnitude over the potential range of 0.30 to -0.30 V when compared to the cases of $AgNO_3$ only and in the presence of Ag NPs (Fig. S6A). The structures formed with tyrosine in the electrolyte are shown in Fig. S6B, which consist of large clusters that sparsely cover the electrode when compared to the case with Ag NPs in solution (Fig. 2C). There is some evidence of dendritic growth but not the type of intertwined structures seen when the Ag NPs are present. Further support of the role of metal NPs in this process rather than any tyrosine that may be present is given by the morphology of the structures formed when Ag is electrodeposited in the presence of Au NPs (Fig. S7). In this case a complex electrode surface, consisting of an array of intertwined dendritic structures are formed. Clearly the composition of the impacting nanoparticle influences the growth process as Ag electrodeposition on Ag is likely to be different to Ag deposition on Au given the substrate dependent nature of electrodeposition.[10] Furthermore the metal deposition peak potential values shift by a similar amount of 140 and 160 mV for Ag and Au in the presence of 1 mM Ag and Au NPs respectively, indicating that the physical blocking effect is the likely cause as opposed to any capping agent effect where the latter severely impacts on the deposition process (Fig. S6A). The presence of KNO_3 supporting electrolyte was also considered, however its inclusion resulted in nanoparticle aggregation and therefore was not studied further.

We then explored the applicability of these materials for the electrochemical oxidation of hydrazine in 1 M NaOH which is a model electrocatalytic reaction as well as being important for fuel

cell applications and sensing where its detection is important due its carcinogenic properties.[3c, 11] Figs. 2E and F show the electro-oxidation of hydrazine at all Ag and Au nanostructures respectively fabricated in this study (Fig. 1). It should be noted that the data is normalised to the electrochemically active surface area of the materials and calculated by Pb underpotential deposition (UPD) and stripping experiments (Fig. S8).[3c, 12] This was particularly important for the Ag system as calculating the area via analysis of the charge associated with oxide reduction is unreliable due to Ag dissolution. It can be seen clearly that the dendritic structures obtained using 500 μM and 50 μM Ag-tyr NPs demonstrated enhanced activity in comparison with the other Ag morphologies, which is consistent with previous observations, that this morphology promotes electrocatalytic activity.[2b, 2d, 13] In comparison, the onset potential for hydrazine oxidation at Au nanostructures occurs at a potential of ca. 100 mV more negative than Ag with increased current density. This is not surprising, as Au under alkaline conditions, is an excellent electrocatalyst and is more active than Ag. Moreover, the well dispersed sub 100 nm clusters obtained with 500 μM Au-cit NPs (Fig. 1G) demonstrated the highest specific activity for the electrochemical oxidation of hydrazine indicating that composition and shape are critical parameters for electrocatalytic performance.

Conclusions

We have proposed that electrostatic interactions between negatively charged colloidal Ag and Au nanoparticles and metal ions in solution in conjunction with the applied potential results in the formation of a diverse range of nanostructured materials. Under conditions where attractive electrostatic conditions apply, dendritic structures can be electrodeposited over the electrode surface, whereas for electrorepulsive conditions well isolated nanoparticles are formed. These materials showed electrocatalytic activity which is dependent on the composition and morphology of the materials. This proof of concept of using nanoparticle collisions as a seeding process for nanostructured growth could in principle be employed for a wide range of other materials with interesting applications.

Acknowledgements

AOM gratefully acknowledges funding from the Asian Office of Aerospace Research and Development (FA2386-13-1-4073) and the Australian Research Council (Future Fellowship - FT110100760).

Notes and references

[a] *School of Applied Sciences, RMIT University, GPO Box 2476V, Melbourne, Australia;*

[b] *School of Chemistry, Physics and Mechanical Engineering, Queensland University of Technology, 2 George St, GPO Box 2434, Brisbane, Queensland, Australia. Email: anthony.omullane@qut.edu.au.* Electronic Supplementary Information (ESI) available: Experimental details, SEM images of control materials and Pb underpotential deposition for surface area determination. See DOI: 10.1039/c000000x/

1(a) C. T. Campbell, *Acc. Chem. Res.*, 2013, **46**, 1712; (b) Y. Huang, H. Ma, S. Wang, M. Shen, R. Guo, X. Cao, M. Zhu and X. Shi, *ACS Appl. Mater. Interf.*, 2012, **4**, 3054; (c) Y. Li and G. A. Somorjai, *Nano Lett.*, 2010, **10**, 2289; (d) R. Sardar, A. M. Funston, P. Mulvaney and R. W. Murray, *Langmuir*, 2009, **25**, 13840; (e) S. E. Kleijn, S. C. Lai, M. T. Koper and P. R. Unwin, *Angew. Chem. Int. Ed.*, 2014, **53**, 3558; (f) A. P. O'Mullane, *Nanoscale*, 2014, **6**, 4012; (g) A. Pearson, H. Zheng, K. Kalantar-zadeh, S. K. Bhargava and V. Bansal, *Langmuir*, 2012, **28**, 14470; (h) E. C. Le Ru and P. G. Etchegoin, *Ann. Rev. Phys. Chem.*, 2012, **63**, 65; (i) P. R. Selvakannan, R. Ramanathan, B. J. Plowman, Y. M. Sabri, H. K. Daima, A. P. O'Mullane, V. Bansal and S. K. Bhargava, *Phys. Chem. Chem. Phys.*, 2013, **15**, 12920; (j) P. C. Ray, *Chem Rev.*, 2010, **110**, 5332; (k) K. Saha, S. S. Agasti, C. Kim, X. Li and V. M. Rotello, *Chem Rev.*, 2012, **112**, 2739.

2(a) G. Zhu, Y. Jiang, F. Lin, H. Zhang, C. Jin, J. Yuan, D. Yang and Z. Zhang, *Chem. Commun.*, 2014; (b) K. A. Homan, J. Chen, A. Schiano, M. Mohamed, K. A. Willets, S. Murugesan, K. J. Stevenson and S. Emelianov, *Adv. Funct. Mater.*, 2011, **21**, 1673; (c) R. Sivasubramanian and M. V. Sangaranarayanan, *CrystEngComm*, 2013, **15**, 2052; (d) A. Pearson, A. P. O'Mullane, S. K. Bhargava and V. Bansal, *Electrochem. Commun.*, 2012, **25**, 87.

3(a) Y. Kim, H. J. Kim, Y. S. Kim, S. M. Choi, M. H. Seo and W. B. Kim, *J. Phys. Chem. C*, 2012, **116**, 18093; (b) J. Solla-Gullon, F. J. Vidal-Iglesias and J. M. Feliu, *Ann. Rep. C*, 2011, **107**, 263; (c) V. Bansal, V. Li, A. P. O'Mullane and S. K. Bhargava, *CrystEngComm*, 2010, **12**, 4280; (d) H. Zhang, J.-J. Xu and H.-Y. Chen, *J. Phys. Chem. C* 2008, **112**, 13886; (e) F. Ye, L. Chen, J. Li, J. Li and X. Wang, *Electrochem. Commun.*, 2008, **10**, 476; (f) N. Tian, Z.-Y. Zhou and S.-G. Sun, *J. Phys. Chem. C*, 2008, **112**, 19801; (g) M. Subhramannia and V. K. Pillai, *J. Mater. Chem.*, 2008, **18**, 5858.

4(a) X. Xiao and A. J. Bard, *J. Am. Chem. Soc.*, 2007, **129**, 9610; (b) X. Xiao, F.-R. F. Fan, J. Zhou and A. J. Bard, *J. Am. Chem. Soc.*, 2008, **130**, 16669; (c) X. Xiao, S. Pan, J. S. Jang, F.-R. F. Fan and A. J. Bard, *J. Phys. Chem. C*, 2009, **113**, 14978; (d) H. Zhou, F.-R. F. Fan and A. J. Bard, *J. Phys. Chem. Lett.*, 2010, **1**, 2671.

5(a) E. J. F. Dickinson, N. V. Rees and R. G. Compton, *Chem. Phys. Lett.*, 2012, **528**, 44; (b) N. V. Rees, Y.-G. Zhou and R. G. Compton, *RSC Adv.*, 2012, **2**, 379; (c) *Chem. Phys. Lett.*, 2012, **525–526**, 69; (d) Y.-G. Zhou, N. V. Rees and R. G. Compton, *Chem. Commun.*, 2012, **48**, 2510; (e) Y.-G. Zhou, E. J. E. Stuart, J. Pillay, S. Vilakazi, R. Tshikhudo, N. V. Rees and R. G. Compton, *Chem. Phys. Lett.*, 2012, **551**, 68.

6 Y.-G. Zhou, N. V. Rees and R. G. Compton, *Angew. Chem. Int. Ed.*, 2011, **50**, 4219.

7 D. Li, J. Liu, C. J. Barrow and W. Yang, *Chem. Commun.*, 2014, **50**, 8197.

8 R. C. Fox, L. T. Nguyen, L. R. Henshaw and L. Yu, *ECS Electrochem. Lett.*, 2013, **2**, H40.

9 M. Y. Lin, H. M. Lindsay, D. A. Weitz, R. C. Ball, R. Klein and P. Meakin, *Nature*, 1989, **339**, 360.

10 B. J. Plowman, S. K. Bhargava and A. P. O'Mullane, *Analyst*, 2011, **136**, 5107.

11(a) H. Zhou, J. H. Park, F.-R. F. Fan and A. J. Bard, *J. Am. Chem. Soc.*, 2012, **134**, 13212; (b) G.-W. Yang, G.-Y. Gao, C. Wang, C.-L. Xu and H.-L. Li, *Carbon*, 2008, **46**, 747; (c) S. E. F. Kleijn, S. C. S. Lai, T. S. Miller, A. I. Yanson, M. T. M. Koper and P. R. Unwin, *J. Am. Chem. Soc.*, 2012, **134**, 18558.

12 Y. Liu, S. Bliznakov and N. Dimitrov, *J. Phys. Chem. C*, 2009, **113**, 12362.

13 W. Ye, J. Yan, Q. Ye and F. Zhou, *J. Phys. Chem. C*, 2010, **114**, 15617.

